Prepared by

Dr Ayodeji Oluleye

Federal University of Technology, Akure, Nigeria

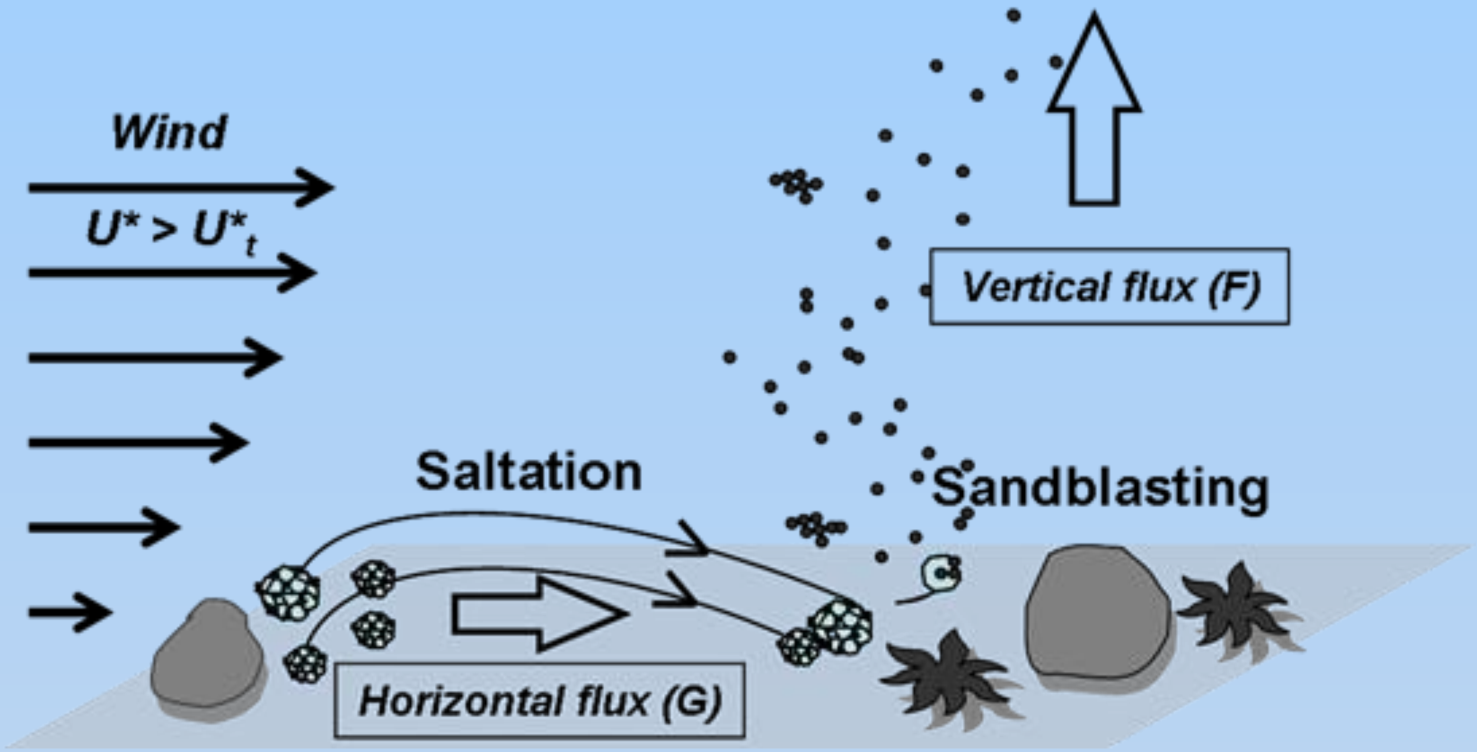

Figure 5.1: Schematic diagram of dust production. The vertical flux is produced during the “sandblasting” process, when the saltating grains (horizontal flux) hit the surface and break the inter-particle bonds linking dust particles together or to the surface. (Figure adapted from Laurent, 2005)

Chapter 5: *Dust* - Lead Author: Peter Knippertz

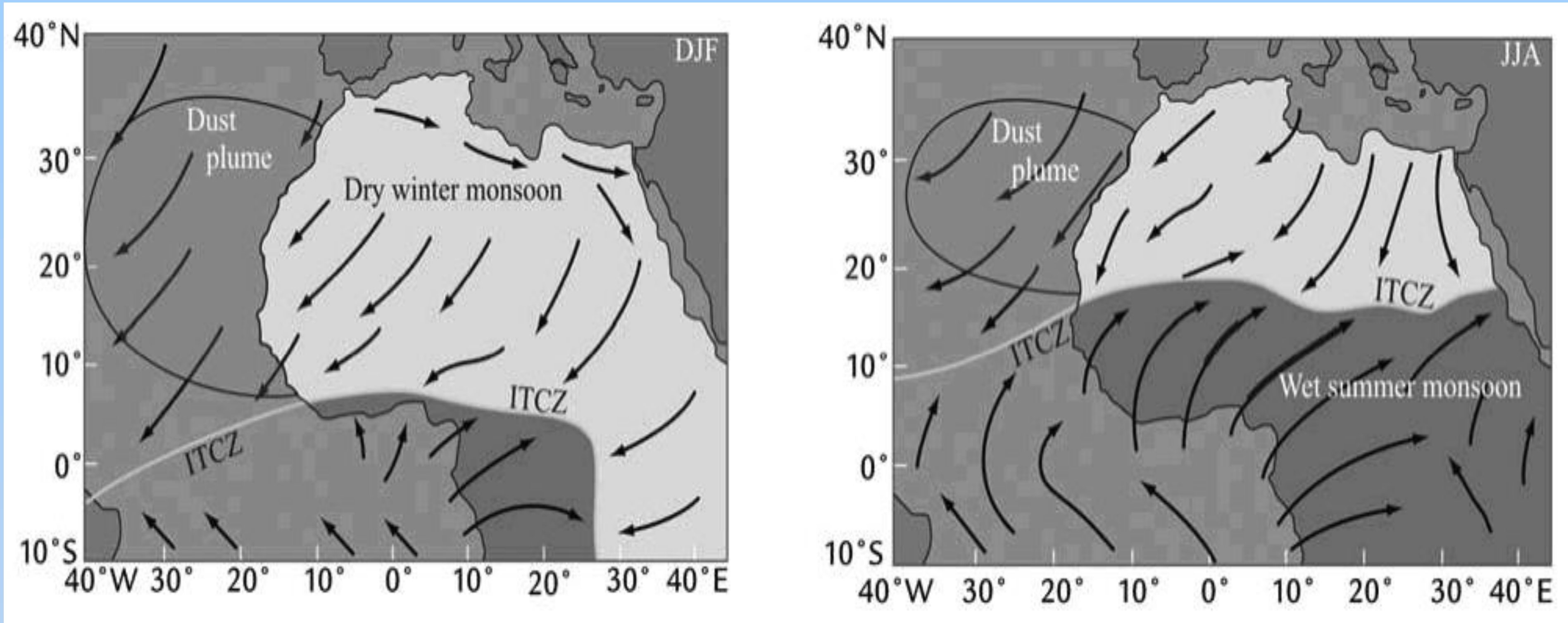

Figure 5.2: Seasonal variation in latitudinal position of the ITCZ and its consequences for atmospheric conditions over northwestern Africa. Arrows indicate direction of trade winds; dust plumes are indicated by grey shadings. December, January, and February (winter) and June, July, and August (summer) are shown. (From Stuut et al., 2005.)

Chapter 5: *Dust* - Lead Author: Peter Knippertz

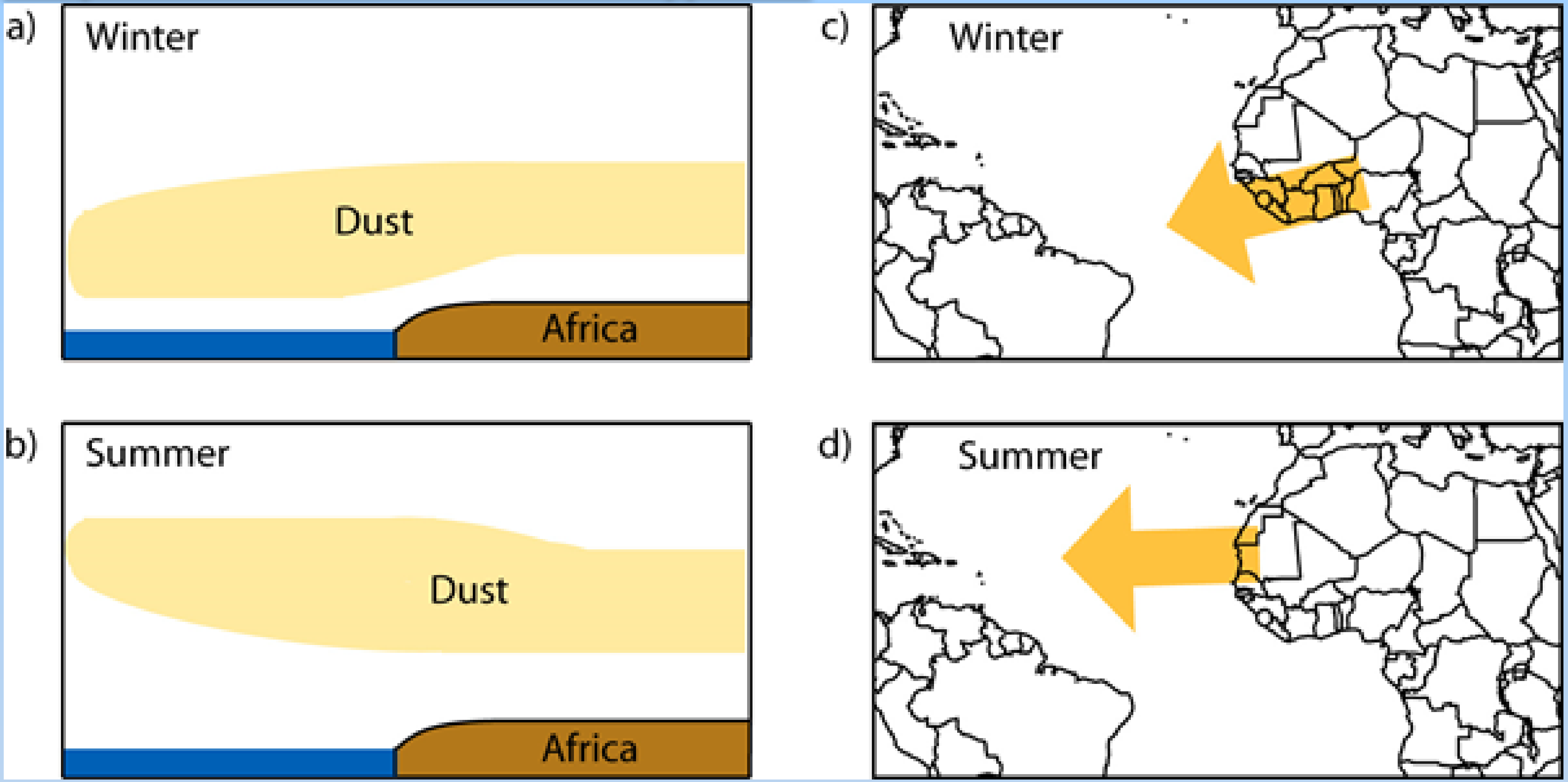

Figure 5.3: Schematic diagram of vertical and horizontal dust export from North Africa towards the tropical East Atlantic for Northern Hemisphere winter (a, c) and summer (b, d).

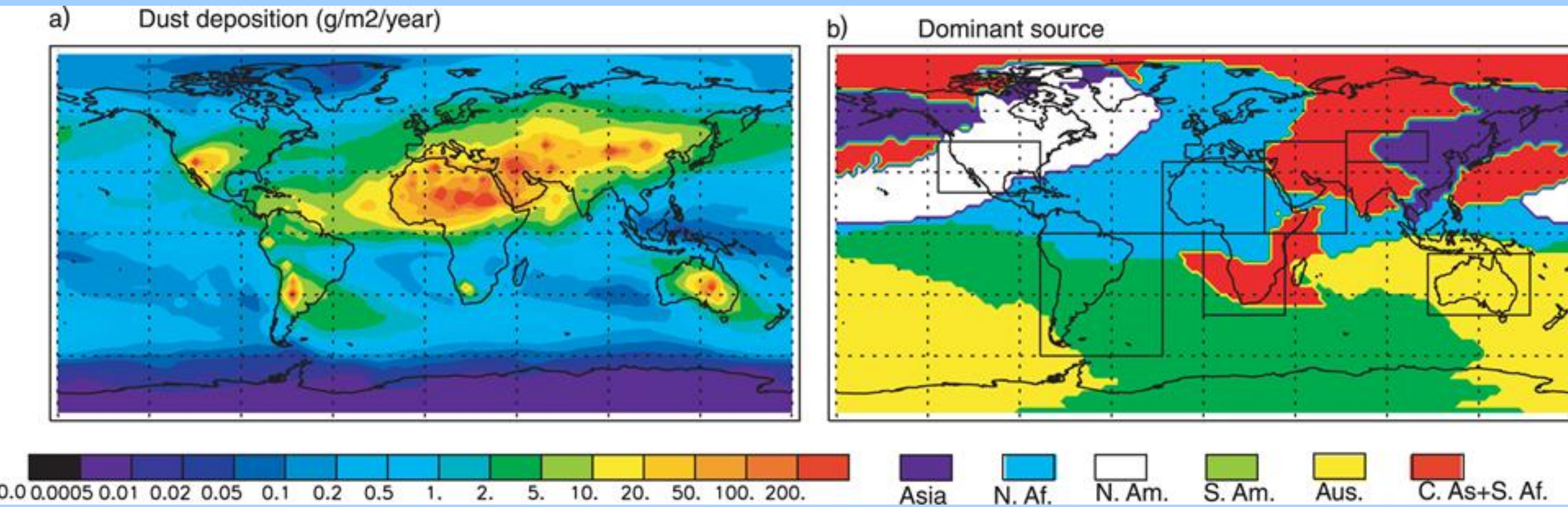

Figure 5.4: (a) Annual deposition fluxes estimated from a dust model. (b) Dominance of source regions for dust deposition indicated by different colours.

(Figures taken from Mahowald, 2007)

African Monsoon Multidisciplinary Analysis

ACMAD

WMO

Chapter 5: *Dust* - Lead Author: Peter Knippertz

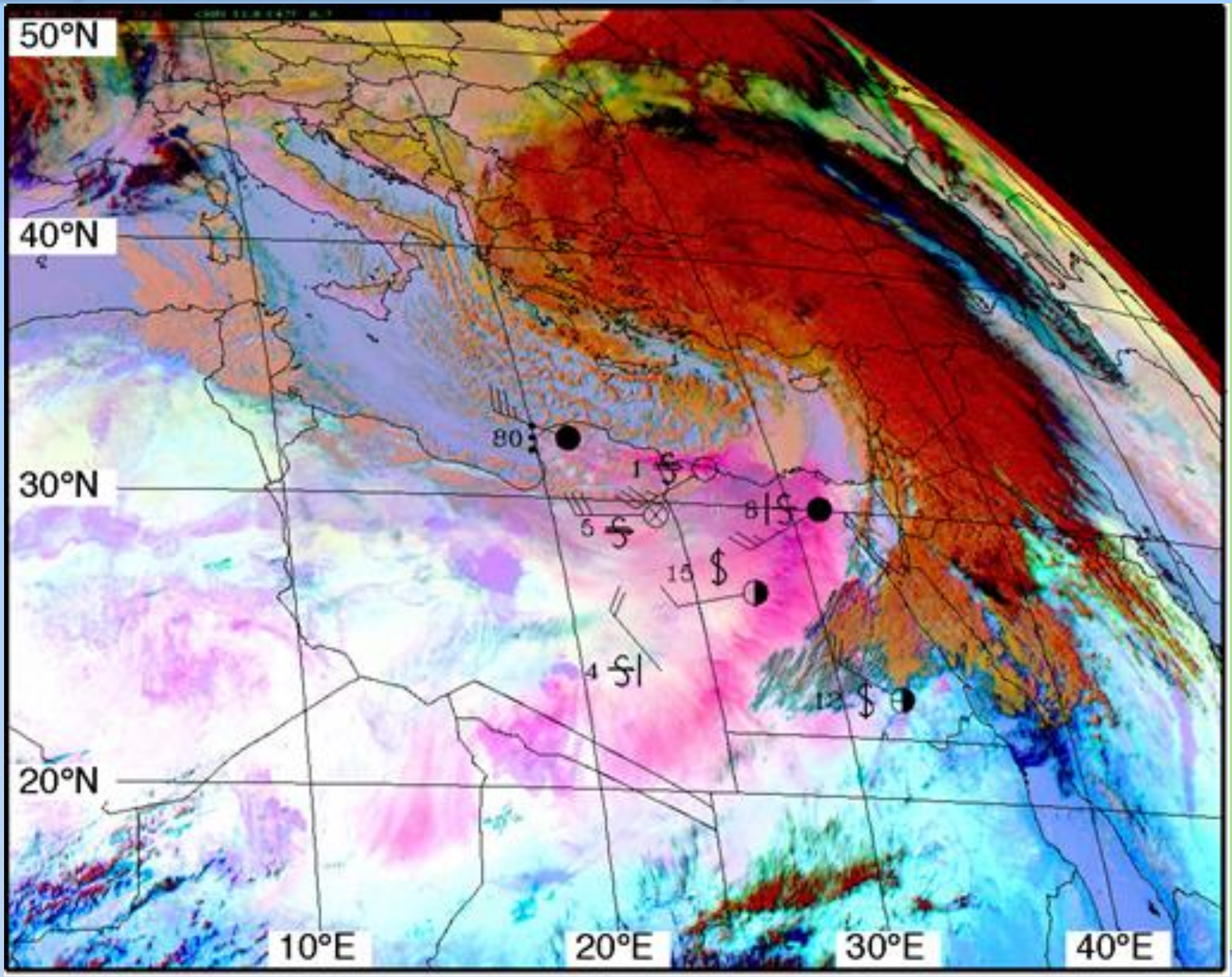

Figure 5.5: Example of an intense Khamsin cyclone over the eastern Mediterranean Sea at 1200 UTC 22 January 2004. The underlying satellite image is a composite of three infrared (IR) channels from the Meteosat Second Generation (MSG) Spinning Enhanced Visible and InfraRed Imager (SEVIRI) instrument. High, optically thick clouds appear red in this image and dust in magenta. The synoptic station reports shown in this Figure indicate severe dust storms with wind speeds of up to 35 kt and a visibility down to 100 m behind the cold front over Egypt and Libya.

(Figure taken from Knippertz and Todd, 2012)

Chapter 5: *Dust* - Lead Author: Peter Knippertz

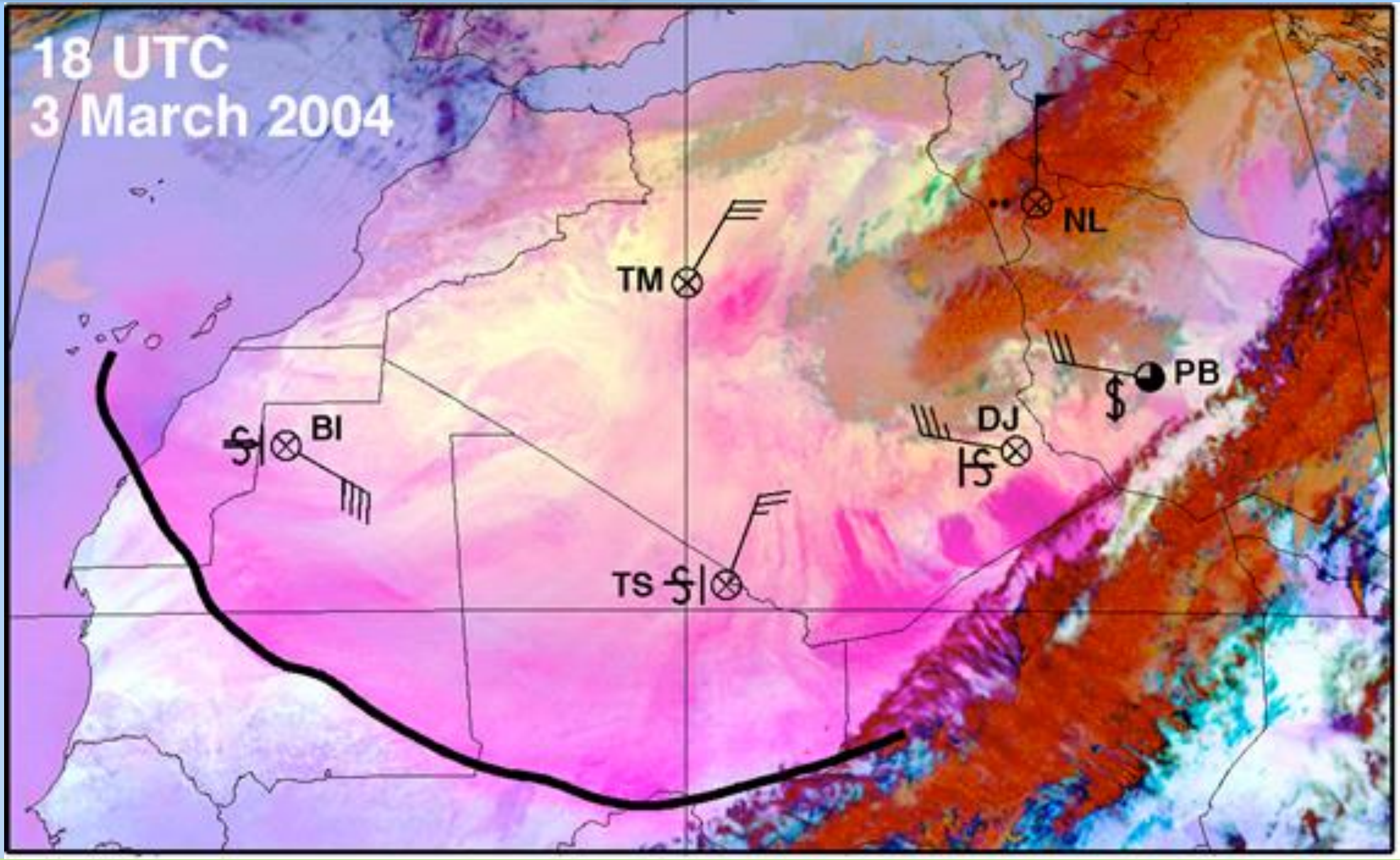

Figure 5.6: Example of an intense large-scale dust outbreak caused by rapid anticyclogenesis over north-western Africa at 1800 UTC 03 March 2004. The underlying satellite image and station reports are as in Figure 5.5. During the following days the dust front continued to spread until it formed a long arc from the Gulf of Guinea to the Canary Islands. See Knippertz and Fink (2006) for more details.

Chapter 5: *Dust* - Lead Author: Peter Knippertz

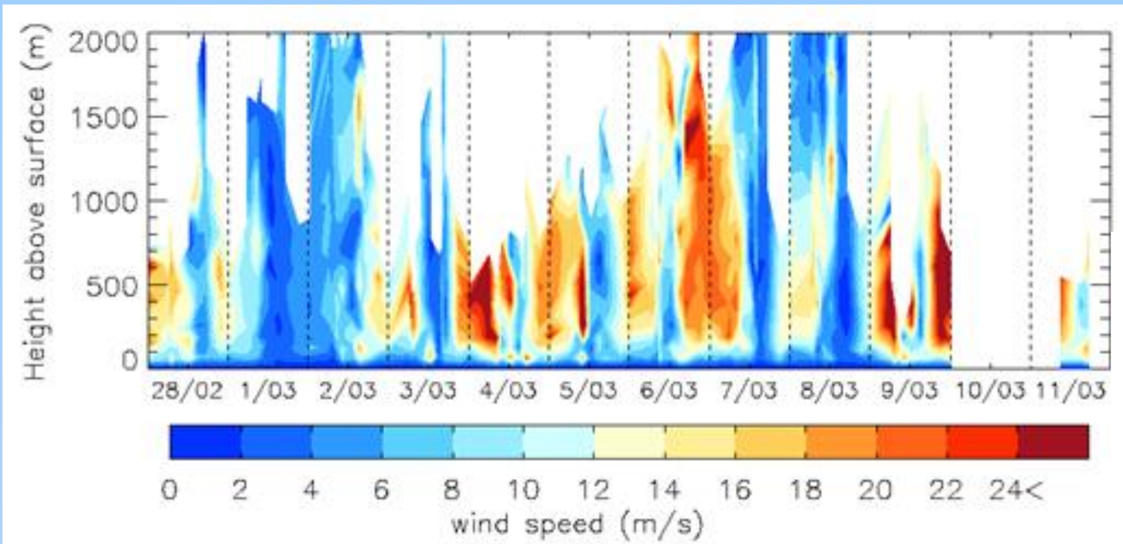

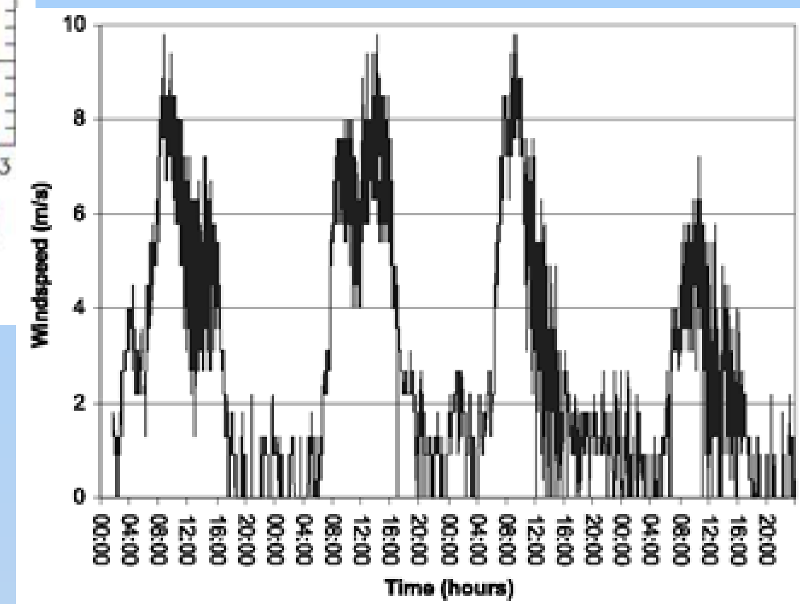

Figure 5.7: Measurements of the effect of nocturnal LLJ formation on surface winds at Chicha (16°53'N, 18°33'E, Chad) during the BoDEx campaign. Left panel: Time-height profile of wind speed from Pilot Balloon data for 28 February to 11 March 2005. Right panel: One-minute averages of 2-m wind speed for 5–8 March 2005. The data show the formation of nocturnal jets and corresponding peaks in surface winds during the morning for some days during the campaign. See also Figure 4.10. (Figures are taken from Washington et al., 2006)

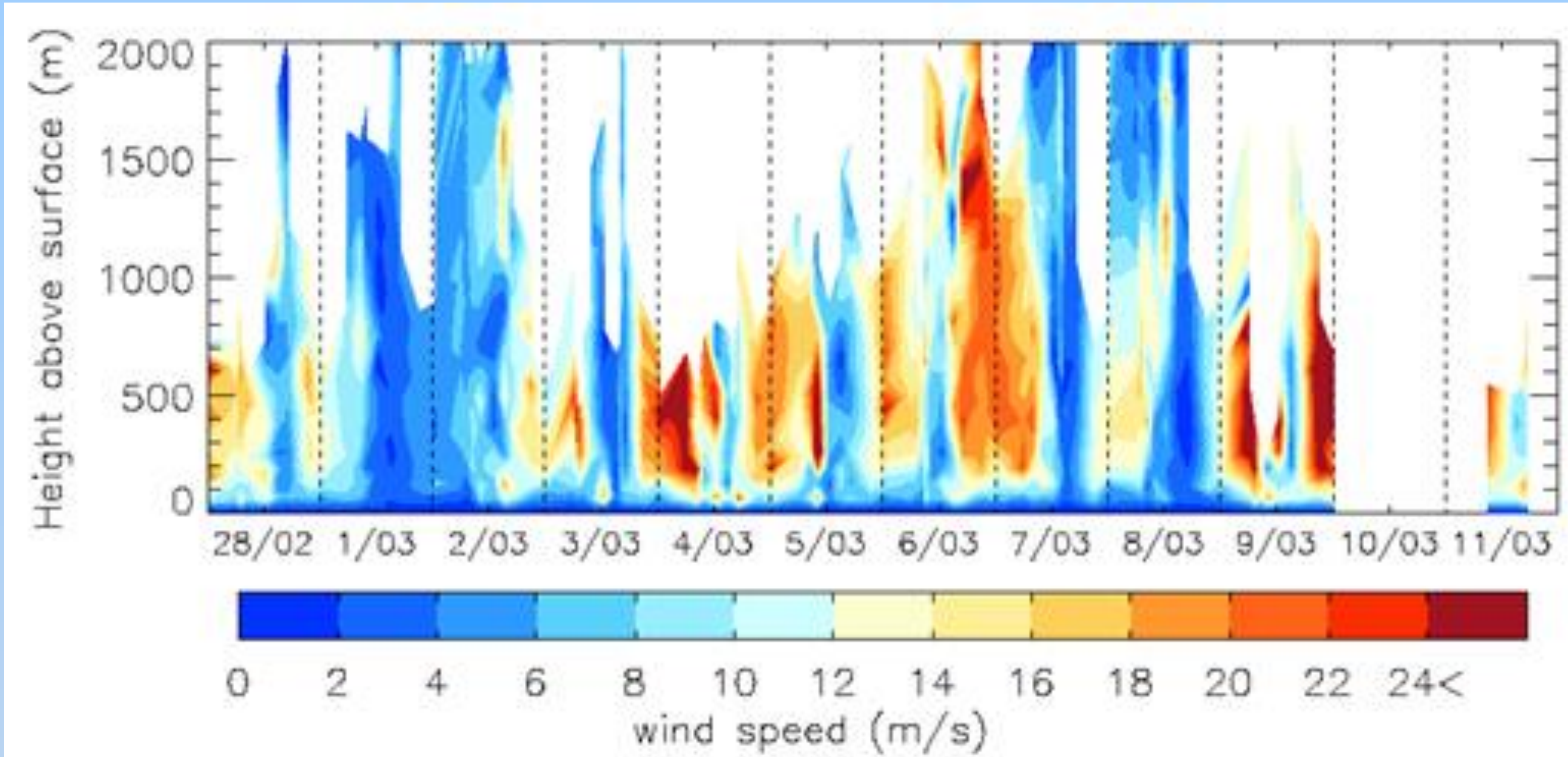

Figure 5.7: Measurements of the effect of nocturnal LLJ formation on surface winds at Chicha (16◦53'N, 18◦33'E, Chad) during the BoDEx campaign. Time-height profile of wind speed from Pilot Balloon data for 28 February to 11 March 2005. The data show the formation of nocturnal jets and corresponding peaks in surface winds during the morning for some days during the campaign. See also Figure 4.10. (Figures are taken from Washington et al., 2006)

Chapter 5: *Dust* - Lead Author: Peter Knippertz

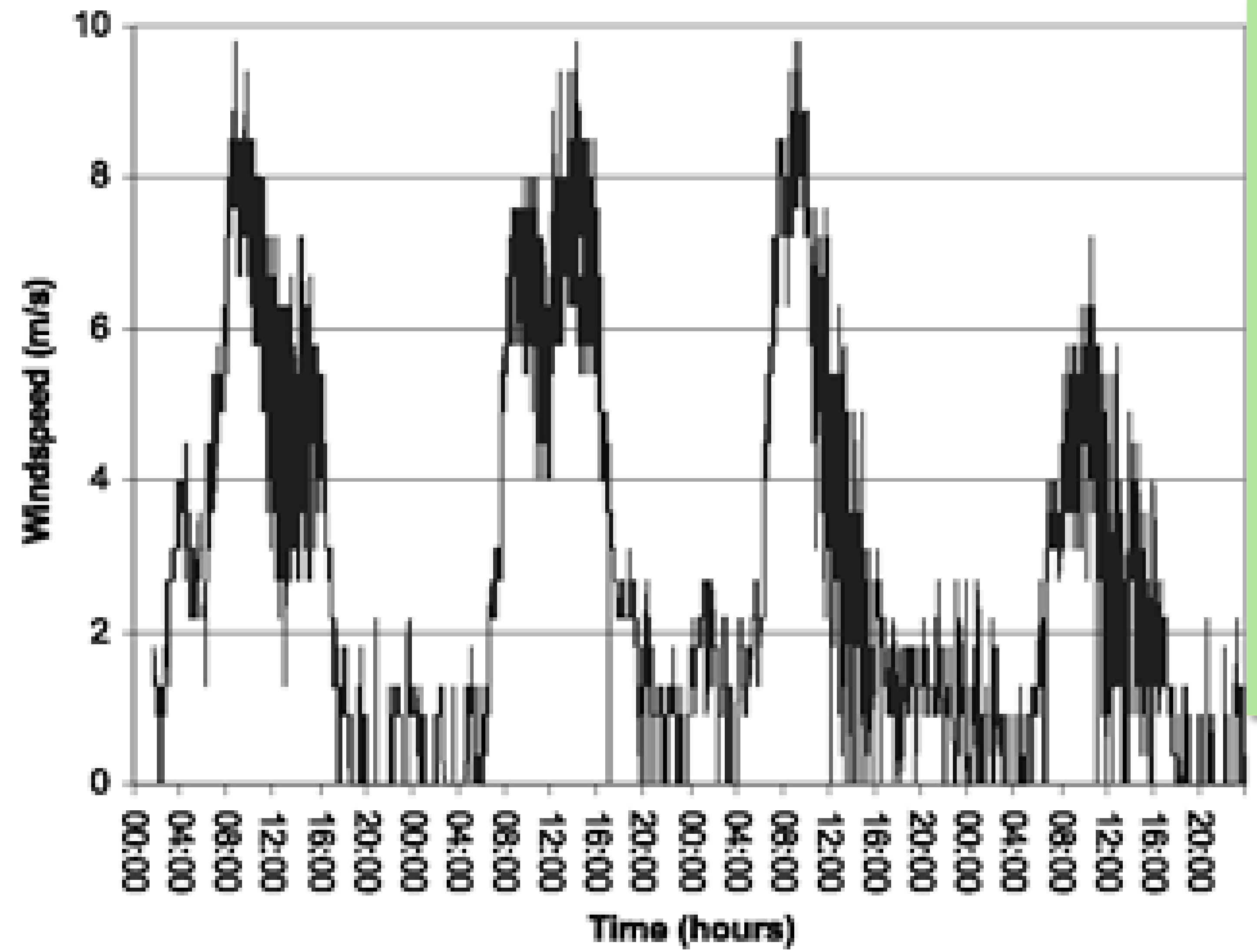

Figure 5.7: Measurements of the effect of nocturnal LLJ formation on surface winds at Chicha (16°53'N, 18°33'E, Chad) during the BoDEx campaign. One-minute averages of 2-m wind speed for 5–8 March 2005. The data show the formation of nocturnal jets and corresponding peaks in surface winds during the morning for some days during the campaign. See also Figure 4.10. (Figures are taken from Washington et al., 2006)

Figure 5.8: Examples of haboob dust storms generated by gust fronts ahead of vigorous squall lines over the Sahel. Upper panel (courtesy of Laurent Labbé): Photograph of a haboob arriving over Niamey on 26 June 2012. Right panels (taken from Williams et al., 2008):

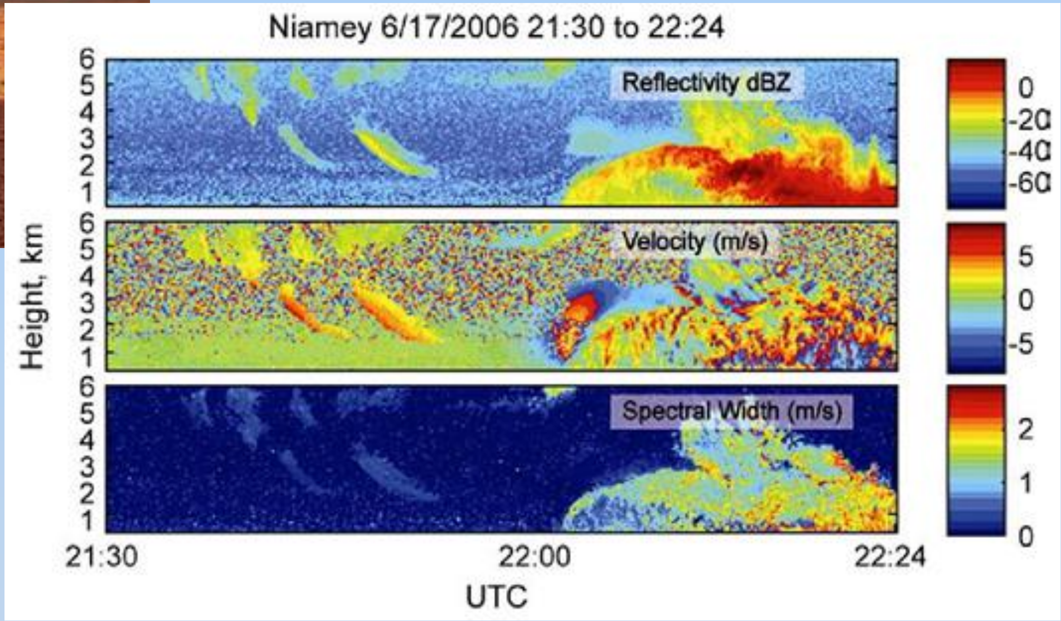

Chapter 5: *Dust* - Lead Author: Peter Knippertz

Figure 5.8: Examples of haboob dust storms generated by gust fronts ahead of vigorous squall lines over the Sahel. (courtesy of Laurent Labbé): Photograph of a haboob arriving over Niamey on 26 June 2012.

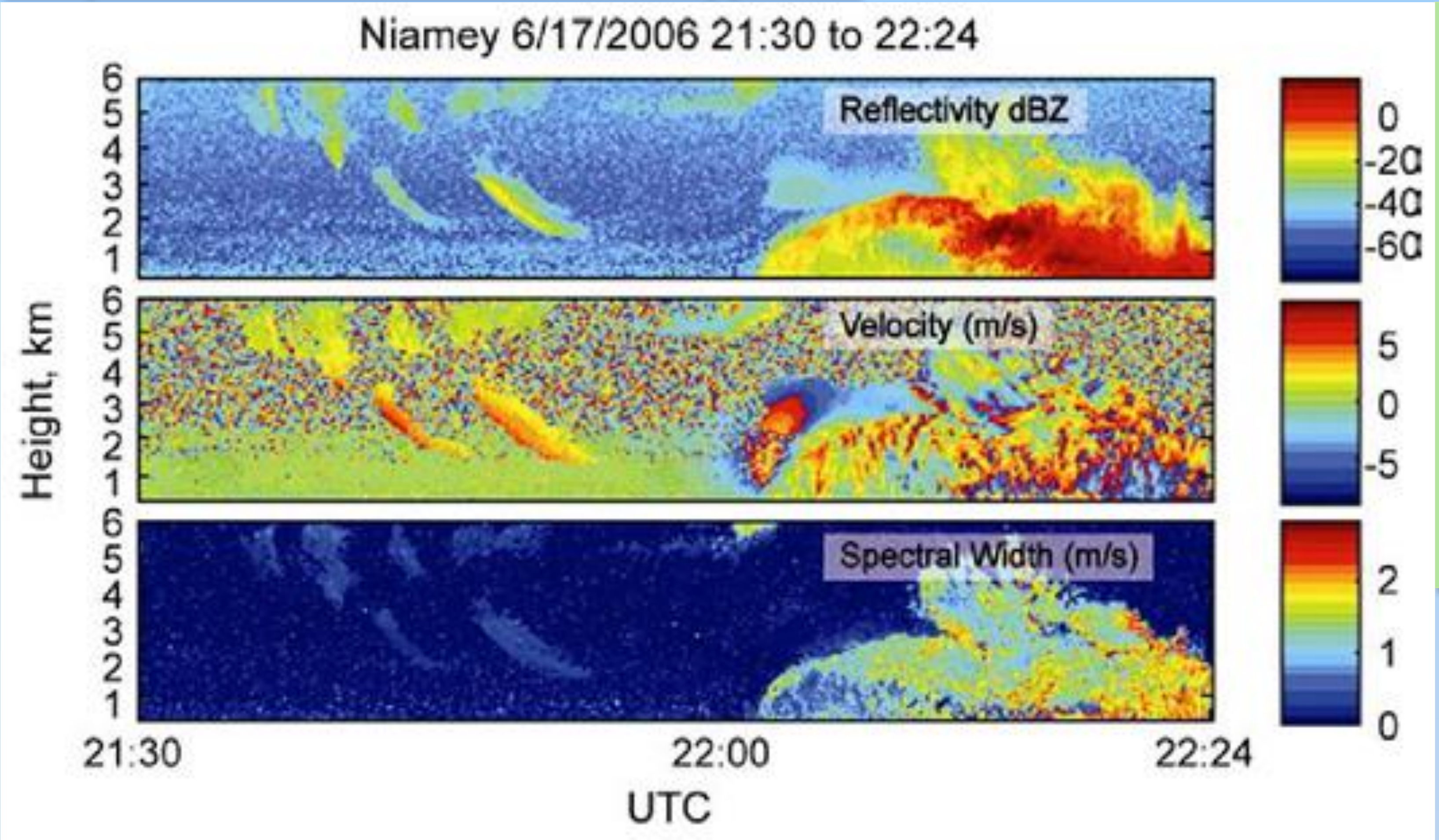

Figure 5.8: Examples of haboob dust storms generated by gust fronts ahead of vigorous squall lines over the Sahel. Right panels (taken from Williams et al., 2008):

Vertical profiles of radar reflectivity, mean Doppler velocity, and Doppler spectral width for a gust front on 17 June 2006 measured with the MIT Doppler radar at Niamey, Niger, at an operating frequency of 95 GHz. Note that insects, sticks and blades of grass are probably the main radar targets, rather than the dust itself.

Chapter 5: *Dust* - Lead Author: Peter Knippertz

Figure 5.9: Examples of (left) a non-rotating dust plume (taken by N. Renno during a 2002 field campaign near Eloy, Arizona, USA, after Koch and Renno, 2005); (right) a rotating dust devil in Tanzania, courtesy of Philippe Peyrillé.

Chapter 5: *Dust* - Lead Author: Peter Knippertz

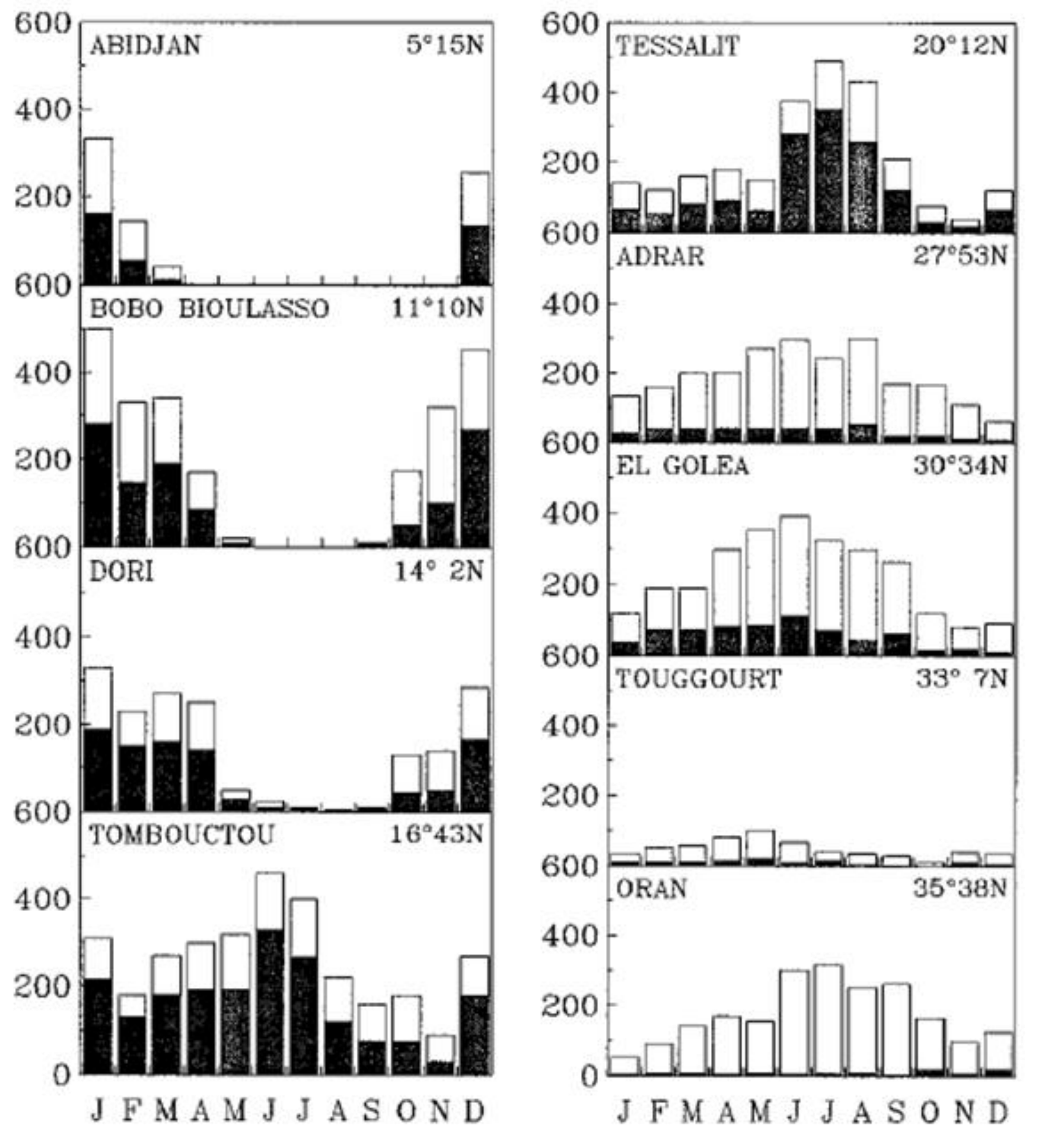

Figure 5.10: Mean monthly number of hours with visibility reduced less than 5 km (shaded bars) and less than 10 km (unshaded bars) during the period 1983–87.

Left: stations from the Guinea coast northward to the central Sahara.

Right: stations from the central Sahara northward to the Mediterranean coast.

Figure taken from Mbourou et al. (1997).

Chapter 5: *Dust* - Lead Author: Peter Knippertz

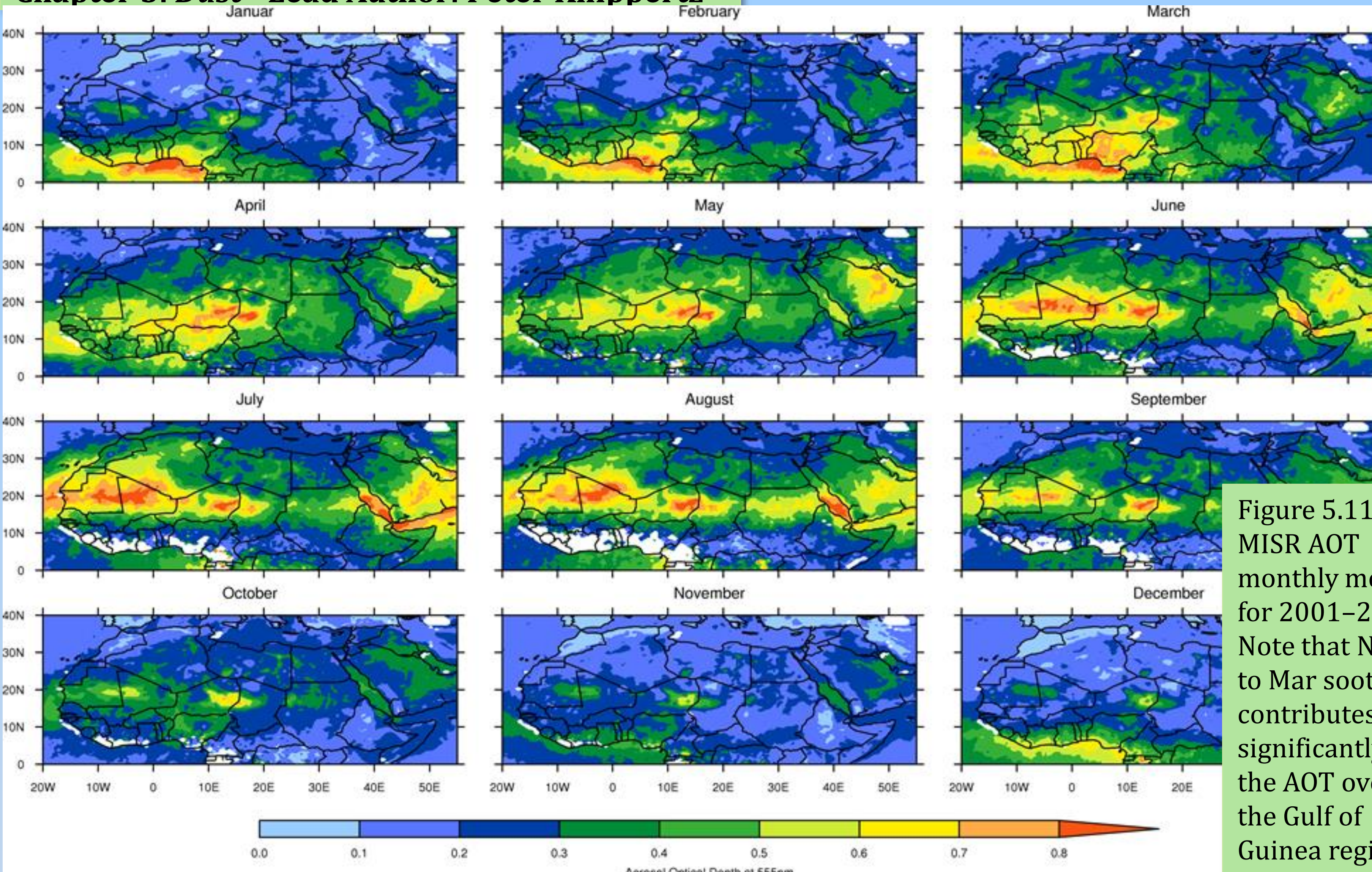

Figure 5.11: MISR AOT monthly means for 2001–2011. Note that Nov to Mar soot contributes significantly to the AOT over the Gulf of Guinea region.

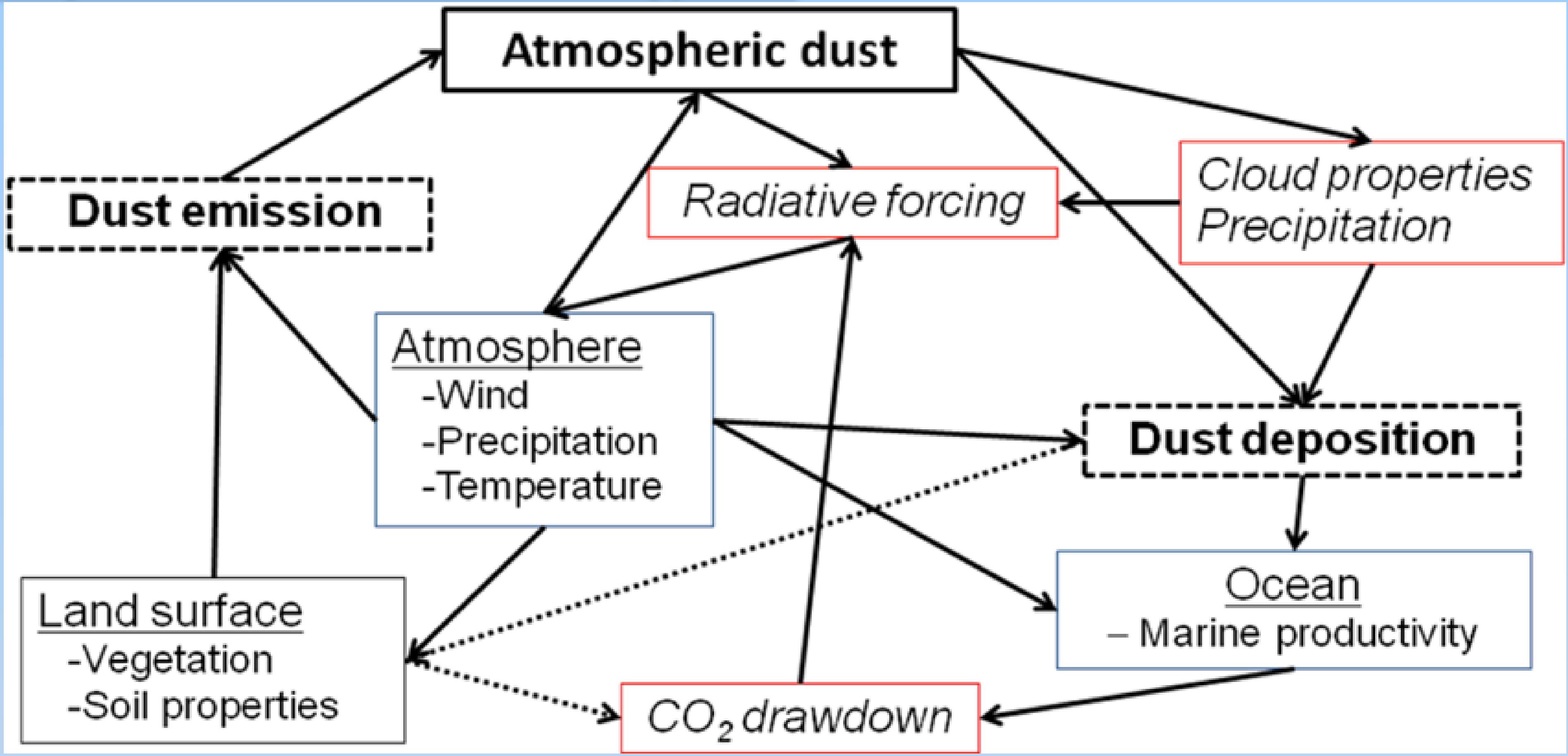

Figure 5.12: Linkages between mineral dust aerosol and climate, indicating direct and indirect aerosol effects, and the role of oceanic dust deposition ecosystems.

Chapter 5: *Dust* - Lead Author: Peter Knippertz

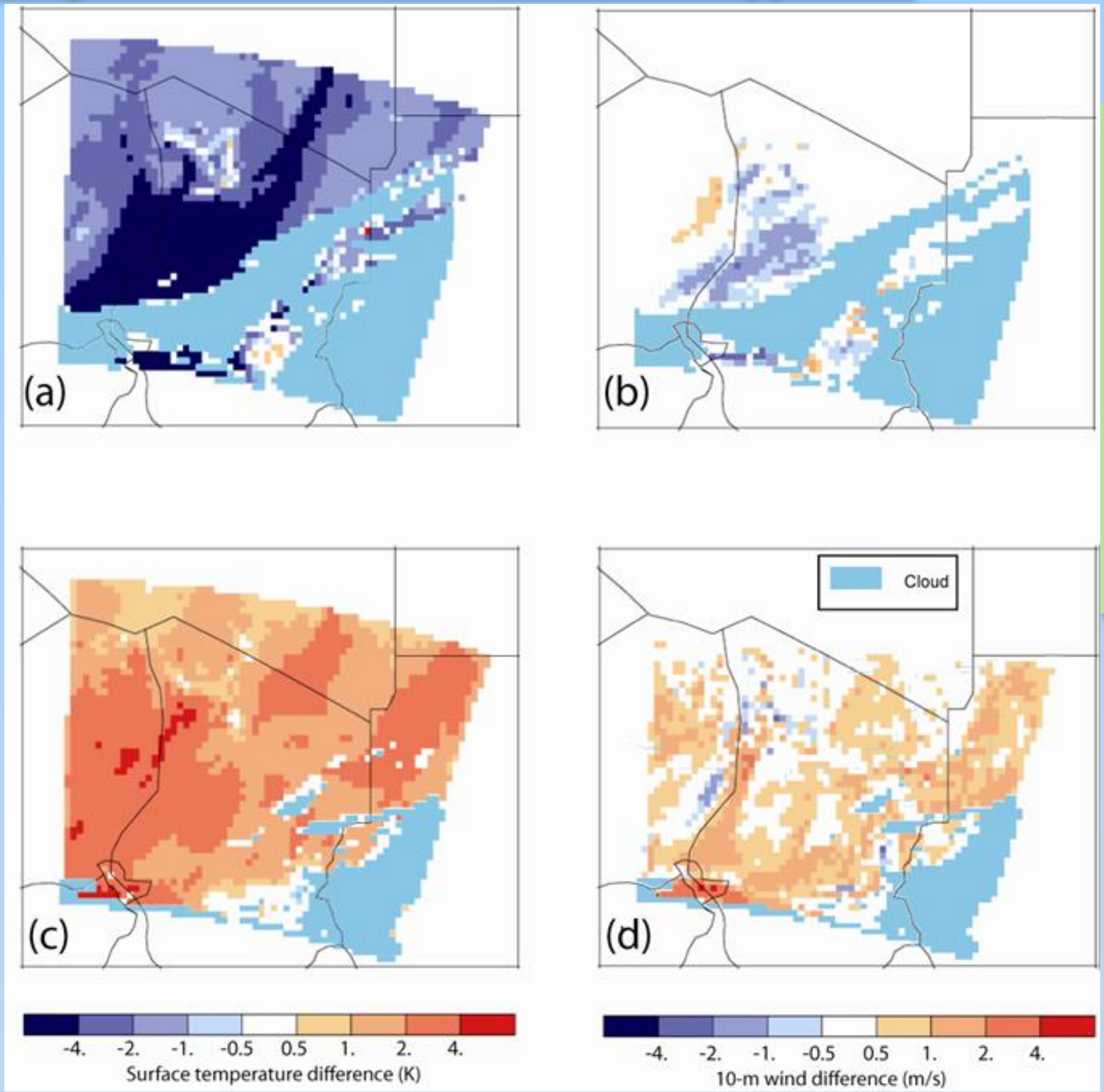

Figure 5.13: Regional model results of changes in 2-m temperatures (a,c) and 10-m wind speeds (b,d) for the Bodélé region in Chad.
The results are shown as difference of the regional model results including dust forcing and results from the model without including dust, on March 11, 2005 for daytime (12 UTC, a,b) and night time (00 UTC) (c,d) conditions.

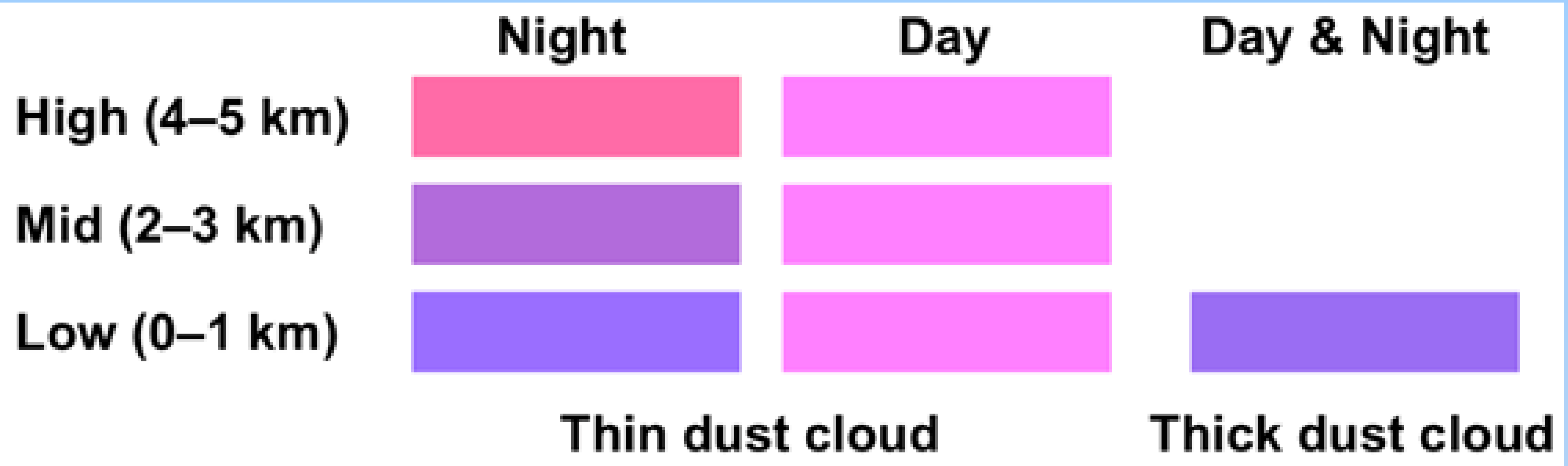

Figure 5.14: Typical appearance of dust clouds in the MSG dust product depending on thickness of the dust cloud, time of day and height.

(based on material from Jochen Kerkmann, EUMETSAT)

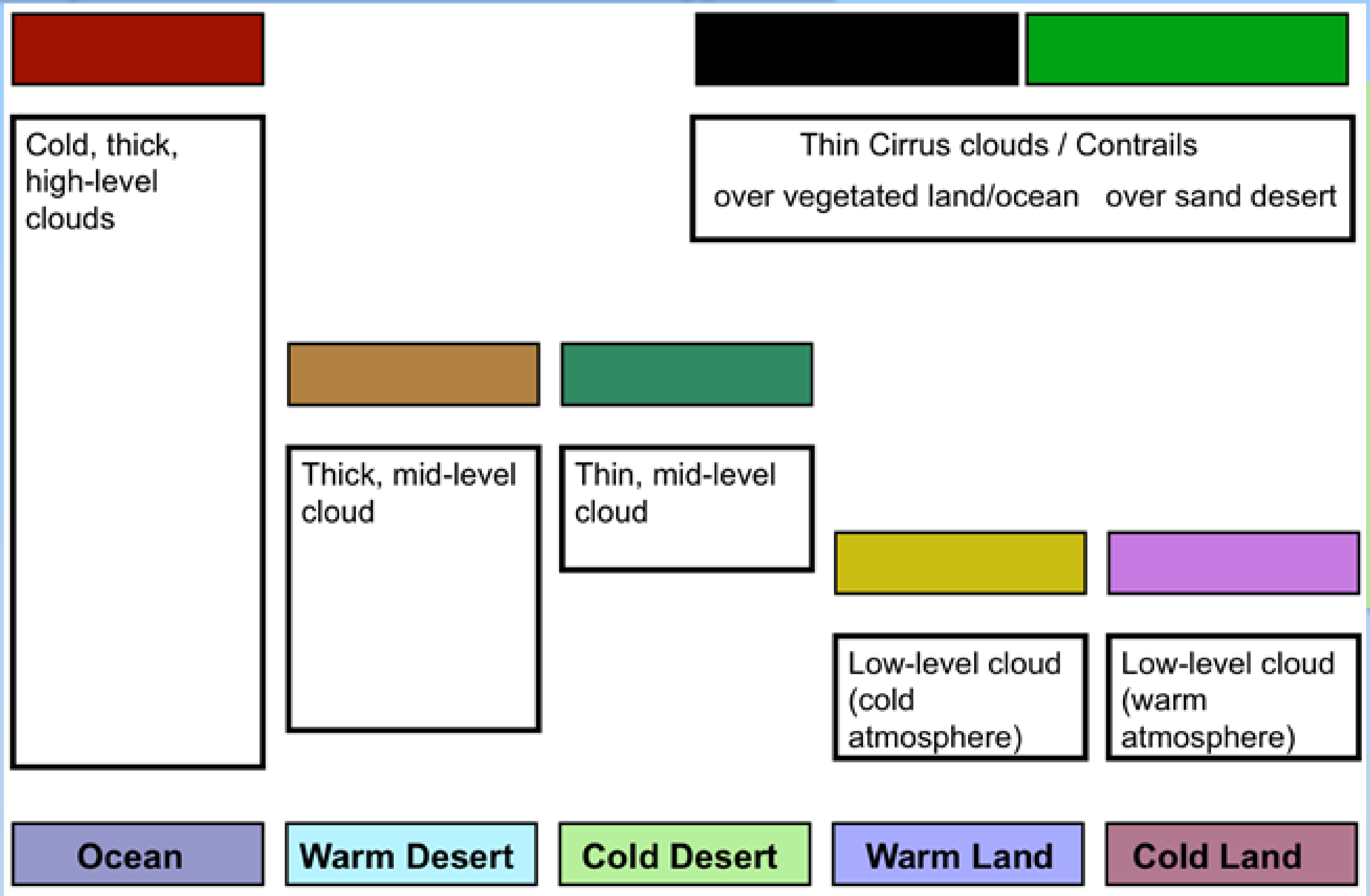

Figure 5.15: Typical appearance of clouds and cloud-free surfaces in the MSG dust product.

(based on material from Jochen Kerkmann, EUMETSAT)

African Monsoon Multidisciplinary Analysis

ACMAD

WMO

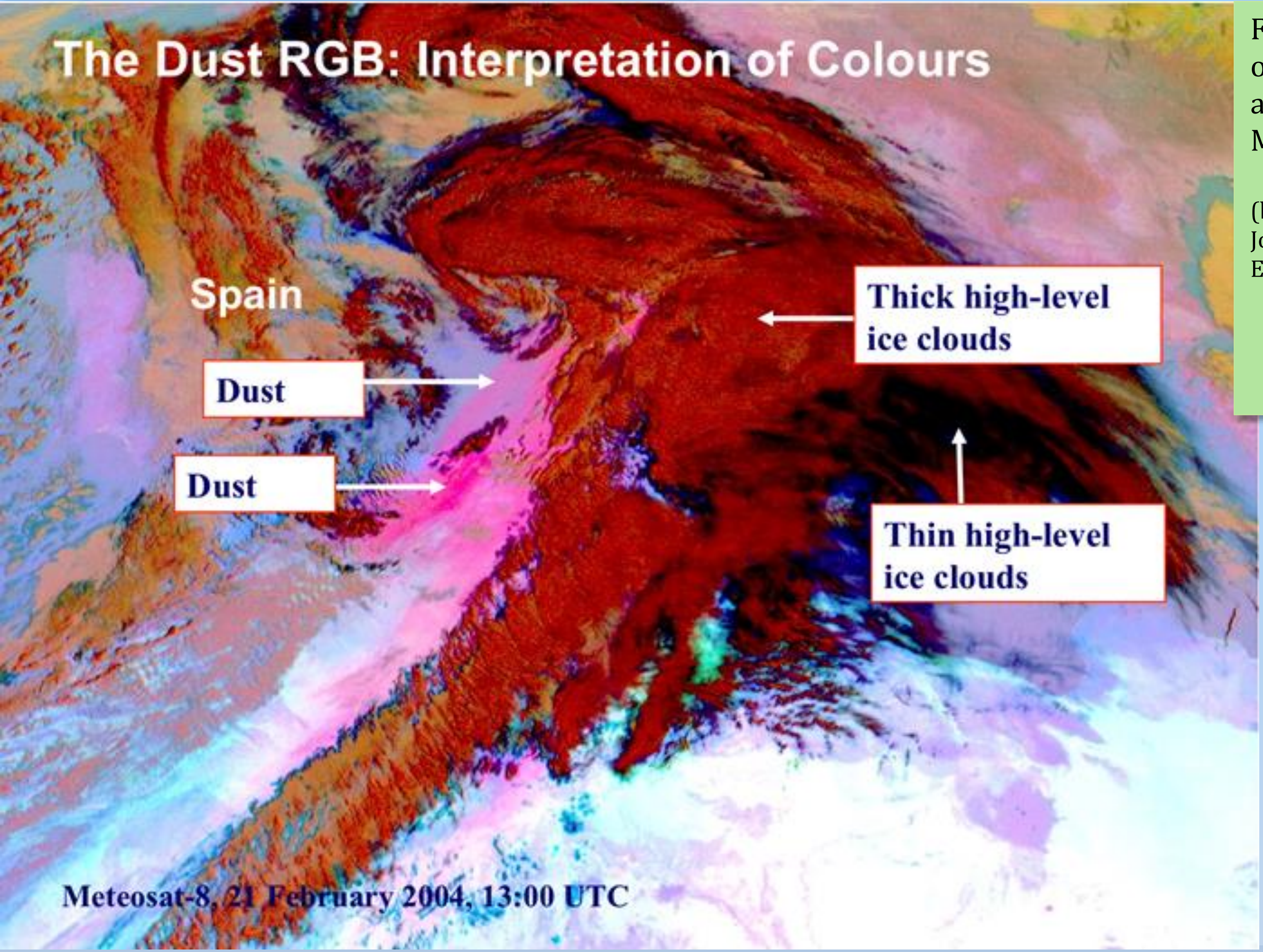

Figure 5.16: Example of the appearance of a dust storm in the MSG dust product.

(based on material from Jochen Kerkmann, EUMETSAT)

Chapter 5: *Dust* - Lead Author: Peter Knippertz

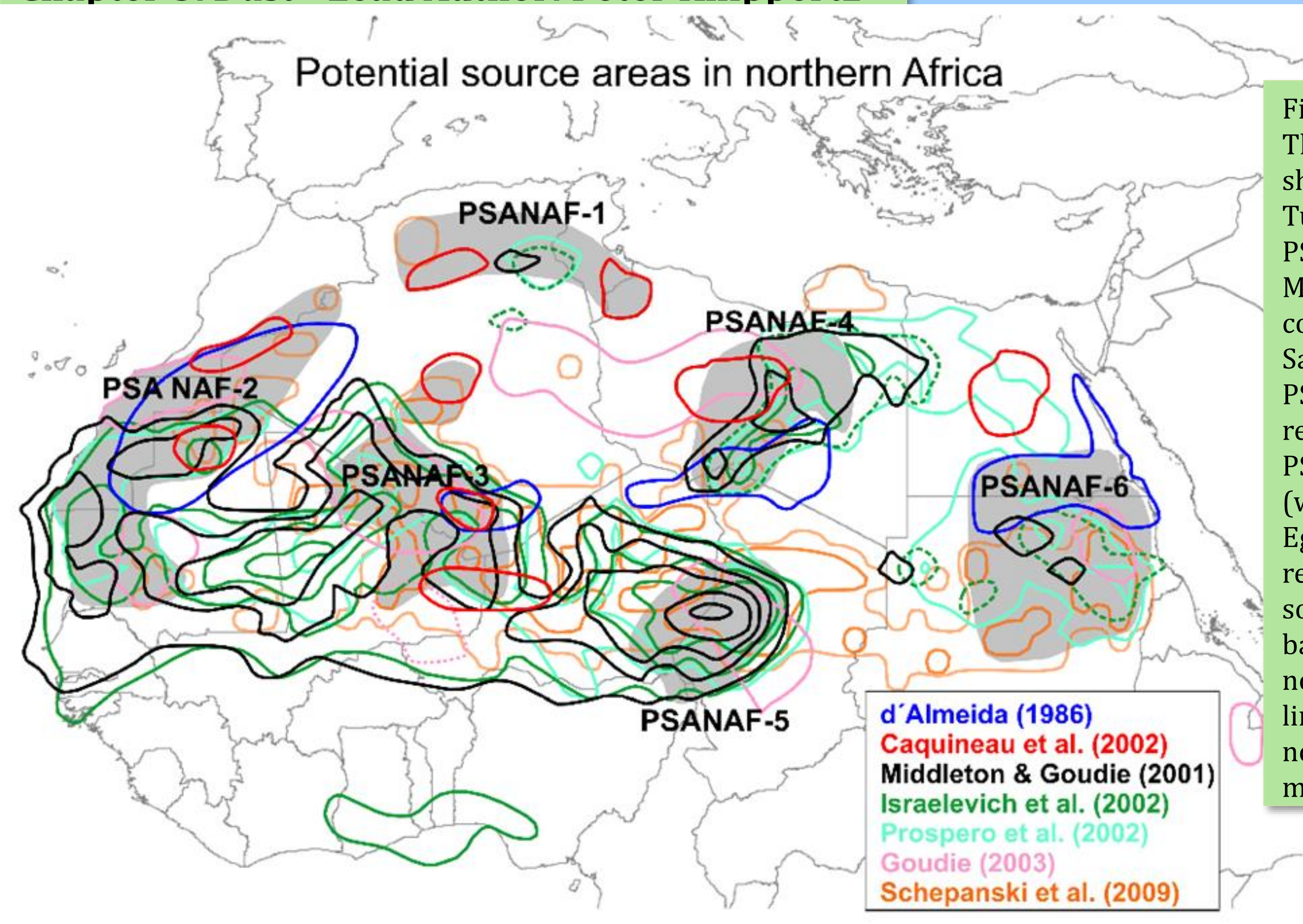

Figure 5.17 contd:
The most important regions are grey shaded: PSANAF-1: Zone of chotts in Tunisia and northern Algeria; PSANAF-2: Foothills of Atlas Mountains (PSANAF-2a) and western coastal region (PSANAF-2b; western Sahara, western Mauritania); PSANAF-3: Mali-Algerian border region; PSANAF-4: Central Libya; PSANAF-5: Bodélé Depression (western Chad); PSANAF-6: Southern Egypt, northern Sudan. Other source regions worth noting are the southern parts of the Azawagh, a dry basin in northwestern Niger / northeastern Mali (pink stippled line), and the Kaouar region in northern Niger (not specifically marked on the Figure).

Figure 5.17: Overview of potential dust source areas in northern hemispheric Africa (PSANAF) based on a synergy analysis by Formenti et al. (2011). The different lines and colours represent analyses by different authors based on different data and techniques (see legend), illustrating the challenge of identifying dust sources with great accuracy.

African Monsoon Multidisciplinary Analysis

ACMAD

WMO

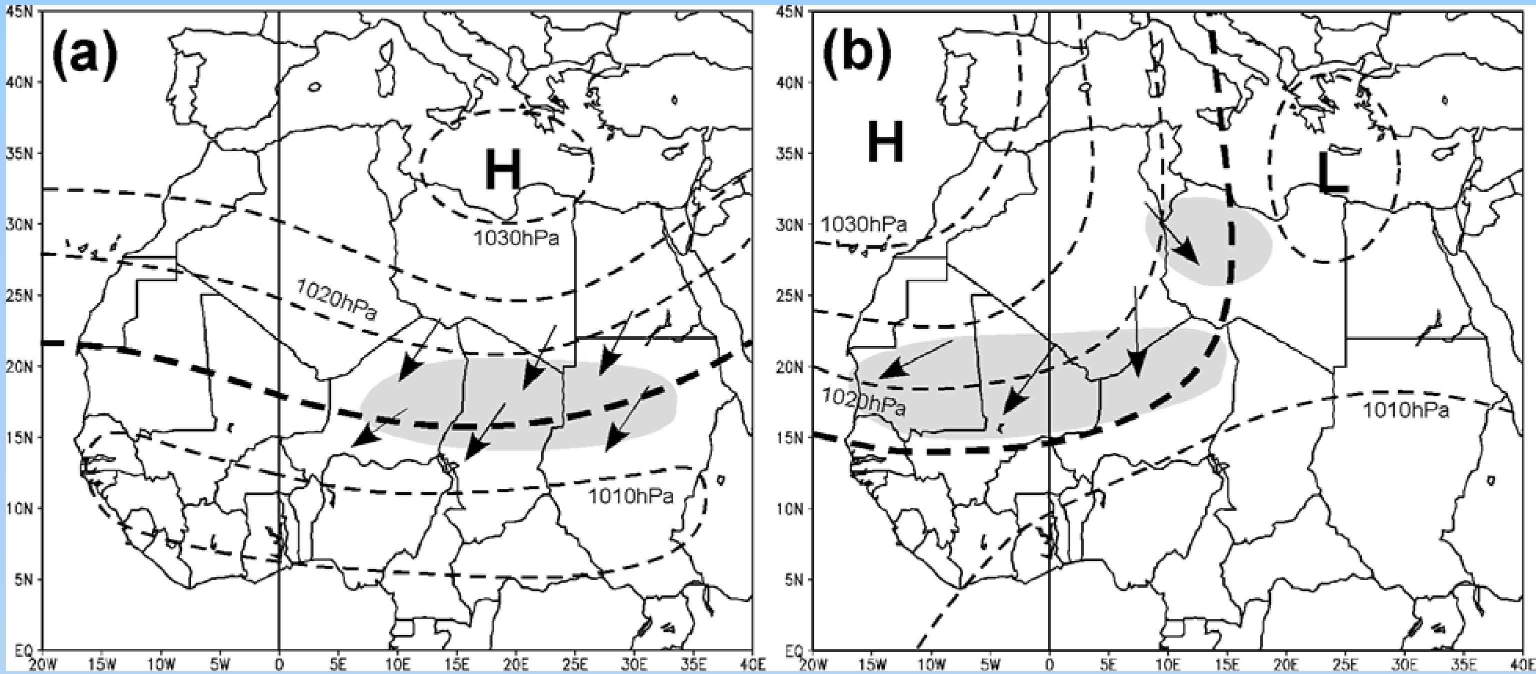

Figure 5.18: Typical situations for the raising of dust during HDH periods. (a) Intensified Libyan High, (b) intensified / south eastward shifted Azores High accompanied by the passage of an extratropical trough across northern Africa. The dashed lines show typical isobars spaced every 5 hPa with the 1015 hPa highlighted in bold. The arrows mark the regions of strongest 10m winds indicating typical wind directions. The grey areas contain active dust sources. Situation (a) will typically precede a HDH episode in the eastern and central parts of West Africa, while situation (b) is more typical of HDH in the western parts.

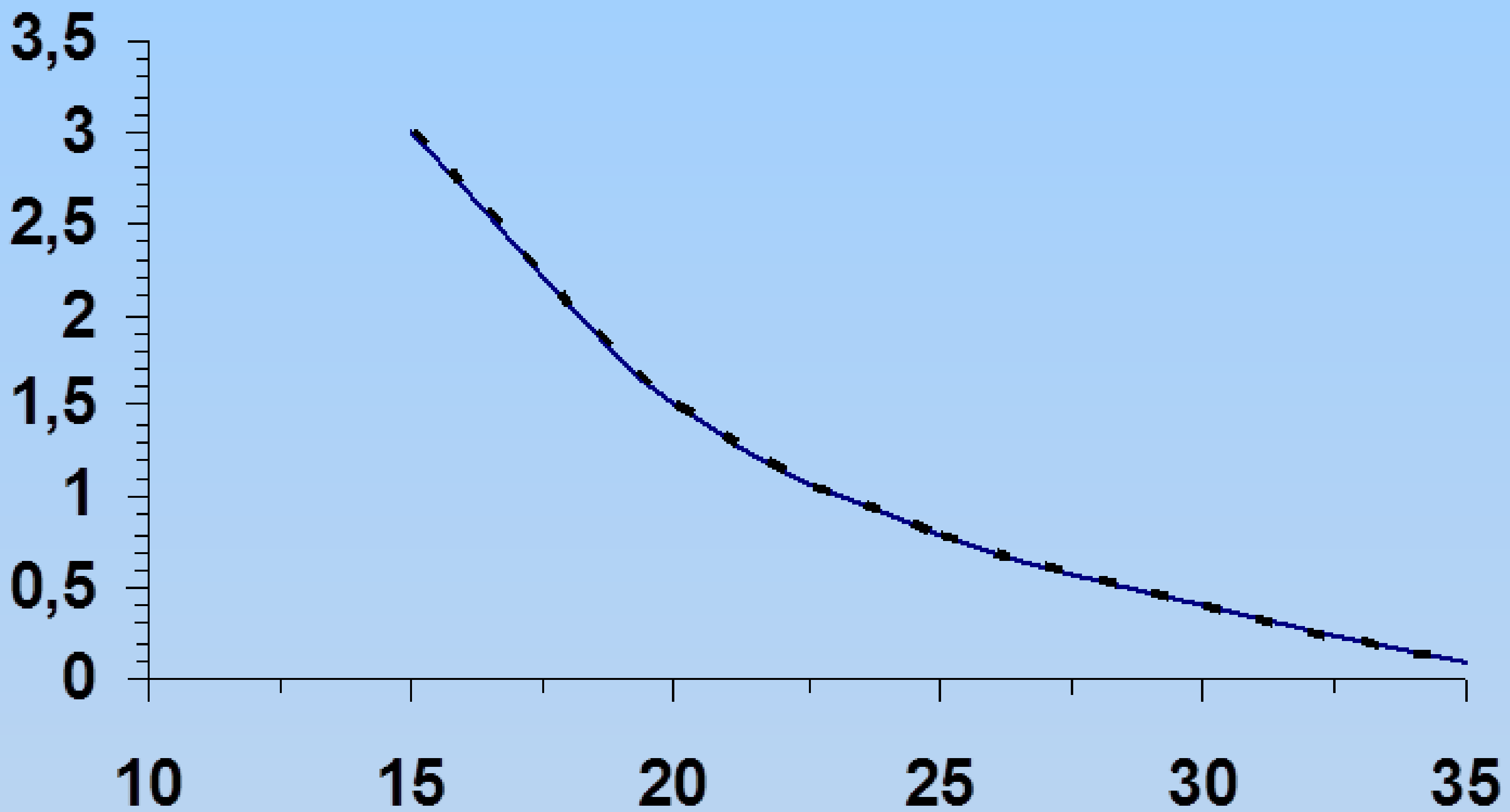

Figure 5.19: Climatological relationship between wind speed (horizontal axis in kt) and horizontal visibility (vertical axis in km) as derived from many Sahelian station observations during different seasons.

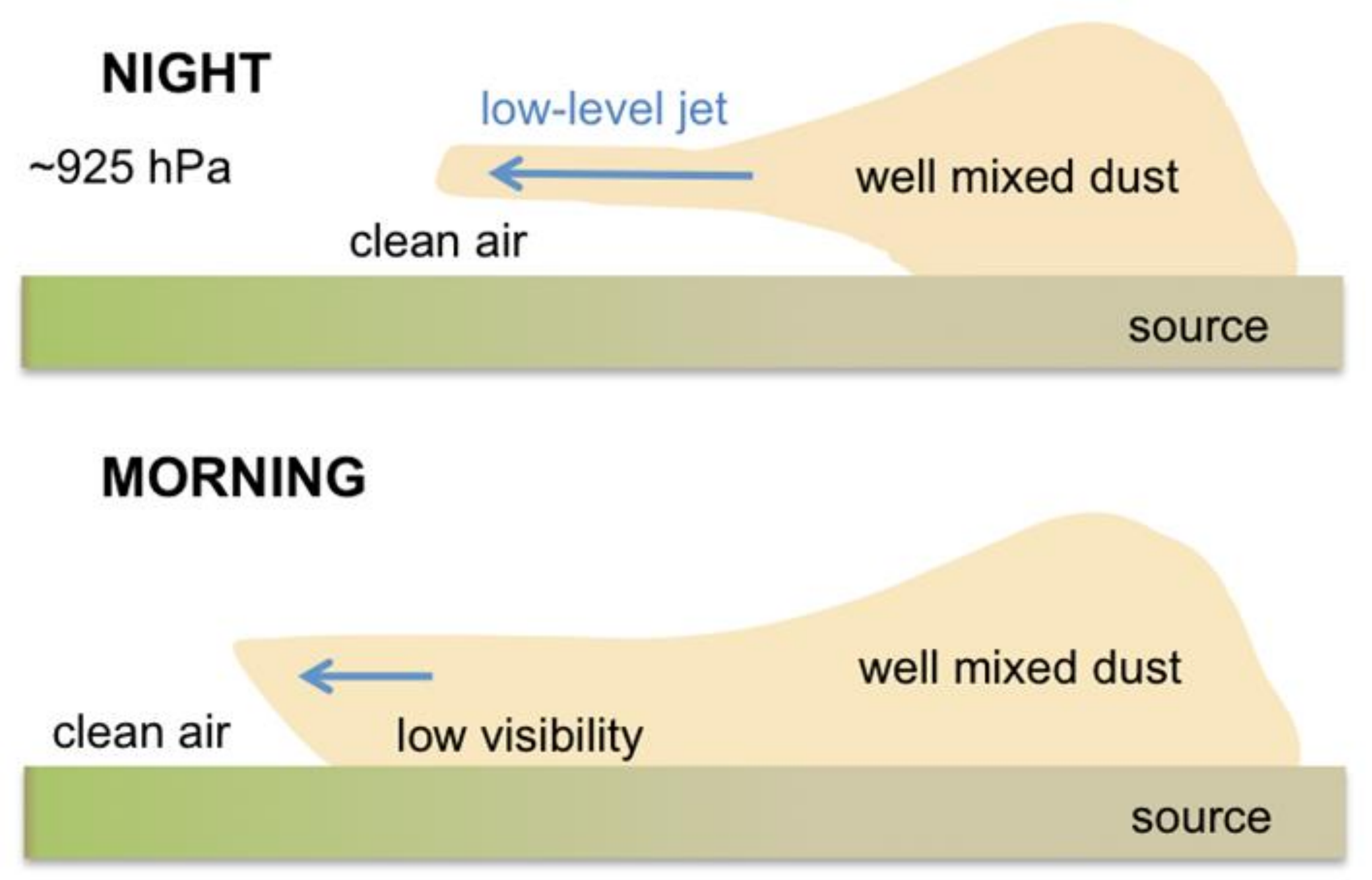

Figure 5.20: Schematic depiction of transport and mixing of dust associated with a nocturnal LLJ.

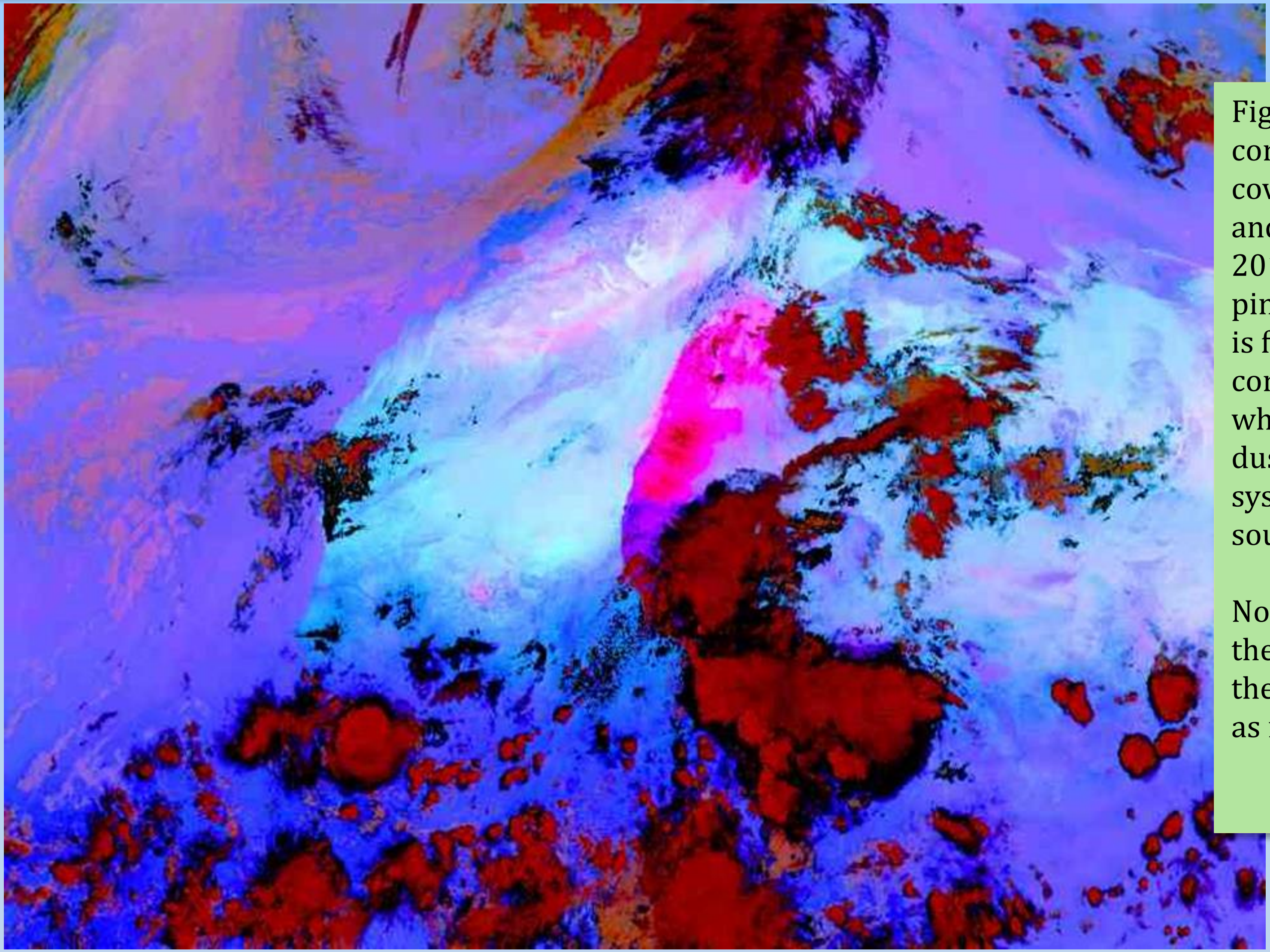

Figure 5.21: Large convective dust storm covering parts of the Sahel and Sahara on 9th June 2010, 173 UTC. The bright pink dust over the Sahara is from a previous convective development, while the darker purple dust is from the convective system to the east and south.

Note that clouds conceal the southern extension of the cold pool into the Sahel, as is often the case.